

RESEARCH

Open Access



Classification of drought severity in contiguous USA during the past 21 years using fractal geometry

Sepideh Azizi^{1,2} and Tahmineh Azizi^{1,2*}

*Correspondence:
tazizi@fsu.edu

¹ Department of Urban and Regional Planning, University of Illinois Urbana-Champaign, Champaign, IL, USA

² Department of Mechanical Engineering, Florida State University, Tallahassee, FL, USA

Abstract

Drought is characterized by a moisture deficit that can adversely impact the environment, economy, and society. In North America, like many regions worldwide, predicting the timing of drought events is challenging. However, our novel study in climate research explores whether the Drought Monitor database exhibits fractal characteristics, represented by a single scaling exponent. This database categorizes drought areas by intensity, ranging from D0 (abnormally dry) to D4 (exceptional drought). Through vibration analysis using power spectral densities (PSD), we investigate the presence of power-law scaling in various statistical moments across different scales within the database. Our multi-fractal analysis estimates the multi-fractal spectrum for each category, and the Higuchi algorithm assesses the fractal complexity, revealing that D4 follows a multi-fractal pattern with a wide range of exponents, while D0 to D3 exhibit a mono-fractal nature with a narrower range of exponents.

Keywords: Fractal geometry, Multi-fractal analysis, Power spectral densities (PSD), Fractal dimension, The Drought Monitor database

1 Introduction

Drought, a natural segment of climate variability, is characterized by prolonged periods of reduced precipitation, affecting various aspects of life and natural resources, including water supplies, businesses, economic stability, social well-being, and the environment [1–6]. The escalating trend of global warming has led to a more frequent occurrence of drought, presenting significant challenges to both humanity and society. This has a profound impact on people's lives, property security, food security, and the availability of water resources [7]. Not only municipal water suppliers could be affected by drought, but also, businesses [1, 2], economic [1], social life and welfare implications [3], and environmental interests which are dependent on wildlife with essential need of precipitation and water [4], may be influenced by drought in the same way [1]. While the USA boasts a robust agricultural system that has historically protected its citizens from severe drought-related impacts, recent droughts have posed significant challenges for farmers across different regions [5].

A typical drought inflicts significant economic losses on American farmers and businesses, ranging from 6 to 8 billion dollars annually. Surprisingly, these financial impacts surpass those incurred from floods and hurricanes. The consequences tend to be even more severe in regions where comprehensive planning for natural hazards is lacking and agriculture serves as the primary economic driver [8]. Various studies have been conducted to assess the relative effects of drought in different parts of the USA, revealing the increasingly apparent impact of drought on human life, wildlife, and agriculture [9–14]. According to these studies, during recent years, we can see clearly the impact of drought on human life, wildlife and agriculture. These studies on different part of the USA which experienced extreme drought discussed that it is likely unprecedented to know about when the next drought will happen. Some predictive models like linear regression have been used to determine the correlation between different factors and the effects of drought in different regions. Many studies have documented increasing the number of drought and severity during recent years in USA which have arisen many new concerns [5, 9, 15–23]. For example, agricultural economic in Nebraska is the first and the most common sector in economic which has been affected adversely by drought [16]. The problem of scarcity of water which happened in the agricultural and energy sectors in a multi-year drought in California (2007–2009) was a reaction to the massive gap between empirical research and the adaptive capacity of social and environmental systems to climate changes [17]. The unprecedented drought in Texas in 2011 led to very dried seasons and intensive wildfires and increasing hardship for ranchers [20, 21]. Climate change in the Pacific Northwest (PNW) of America has caused more frequent droughts, rising air temperature, reducing winter snowfall, increasing earlier snow-melt, reducing summer flows, and longer crop-growing season [23]. In North Carolina, forest ecosystem sectors such as clean water, wildlife habitat, and timber supplies are progressively affected by drought during recent years [9]. Based on these recent records of severe drought impacts in different parts of USA and many more, it is crucial to better understanding the drought features and patterns to decrease the environmental and economical costs and damages.

To track drought conditions and their related environmental factors, resources such as the National Drought Mitigation Center (NDMC), National Oceanic and Atmospheric Administration (NOAA), and the United States Department of Agriculture (USDA) provide valuable information. Early detection of drought allows for proactive measures to reduce its impacts and economic losses. According to the US Drought Monitor (USDM) reports, there are different ways to recognize drought such as comparison between observed precipitation, soil moisture and crop conditions with their regular time and so on. The US Drought Monitor (USDM) is a collaborative effort started from 1999 and produced by the National Drought Mitigation Center (NDMC) at the University of Nebraska-Lincoln, the National Oceanic and Atmospheric Administration (NOAA), and the US Department of Agriculture (USDA).

Drought experts regularly estimate precipitation levels, comparing them to long-term averages, while considering various variables like temperature, soil moisture, water levels in streams and lakes, snow cover, and meltwater runoff. They also identify areas experiencing drought impacts, including water shortages and business disruptions. Experts use multiple indicators to assess regional-scale drought conditions

and consult with other specialists before releasing weekly drought maps known as the US Drought Monitor (USDM) maps, see Fig. 1 (Source(s): National Drought Mitigation Center (NDMC), National Oceanic and Atmospheric Administration (NOAA), United States Department of Agriculture (USDA)).

Figure 1 displays the US Drought Monitor (USDM) categorization, which classifies drought into five levels: (1) D0, indicating areas abnormally dry but not yet in drought or recovering from it; (2) D1, representing moderate drought, the least severe level; (3) D2, marking severe drought; (4) D3, signifying extreme drought; and (5) D4, the most severe level, exceptional drought. This classification is vital for risk assessment and drought management, aiding in the quantification and evaluation of potential issues [Source(s): National Drought Mitigation Center (NDMC), National Oceanic and Atmospheric Administration (NOAA), United States Department of Agriculture (USDA)].

Various indices are employed to assess drought severity and its impacts across different timescales, including widely recognized measures like the Standardized Precipitation Index (SPI) and the Palmer Drought Severity Index (PDSI). These indicators have been utilized in operational drought management for many years, and their characteristics and performance characteristics are well-documented and understood [24]. Another commonly used index for drought monitoring is the Normalized Difference Vegetation Index (NDVI) [25–27]. This index aids in assessing drought severity by tracking variations in vegetation cover within a specific region over a defined time frame. Satellite databases, including data from Advanced Very-High-Resolution Radiometer (AVHRR), Terra Moderate Resolution Imaging Spectroradiometer (MODIS), and Landsat sensors, record and quantify changes in vegetation coverage due to evolving climate conditions. Positive NDVI values indicate vegetated areas, while zero and negative values correspond to bare soil and water bodies [25]. Significant progress has been achieved in understanding the impact of drought on vegetation dynamics by examining the correlations within their response characteristics. Several scientists have assessed vegetation productivity in response to droughts at various

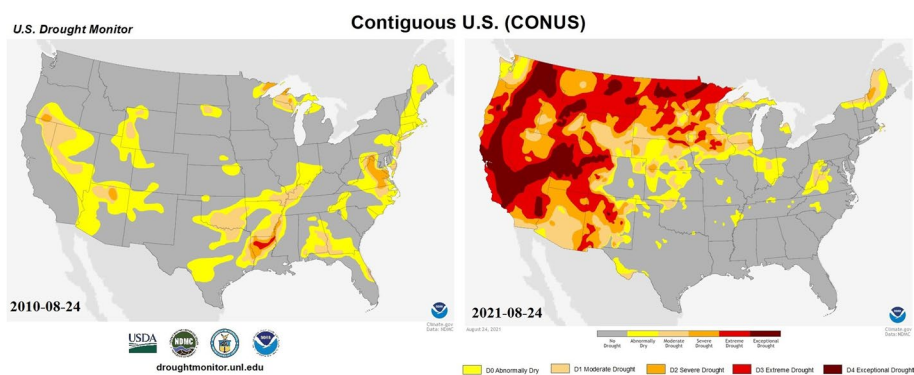


Fig. 1 US Drought Monitor Category (left: 2010-08-24) and (right: 2021-08-24) taken from US Drought Monitor (USDM). The maps use five classifications: abnormally dry (D0), showing areas that may be going into or are coming out of drought, and four levels of drought: moderate (D1), severe (D2), extreme (D3), and exceptional (D4). Map of the USA painted with blobs of yellow, orange, and red, <https://droughtmonitor.unl.edu/CurrentMap/StateDroughtMonitor.aspx?conus>. Source(s): National Drought Mitigation Center (NDMC), the US Department of Agriculture (USDA), and the National Oceanic and Atmospheric Administration (NOAA)

timescales, employing measures such as the 3-, 6-, 12-, and 24-month Standardized Precipitation Evapotranspiration Index (SPEI) and Normalized Difference Vegetation Index (NDVI) [28].

Figure 2 displays the time series of the average NDVI for Arizona, encompassing regions with moderate to exceptional drought (D1–D4), over ten years (2010–2021) for each month. The NDVI data, sourced from the open-source Google Earth Enterprise and derived from Terra Moderate Resolution Imaging Spectroradiometer (MODIS), serves as a valuable resource for predicting future vegetation changes in Arizona.

Each state experiences a different set of impacts during a drought. We have also demonstrated the table of reported impacts during past droughts in Arizona for each level of drought on the US Drought Monitor in Fig. 3 (Source(s): National Drought Mitigation Center (NDMC), National Oceanic and Atmospheric Administration (NOAA), United States Department of Agriculture (USDA)).

When studying real-world time series, one often encounters databases exhibiting non-linear power-law properties, indicative of self-similar or fractal-like patterns across various scales [6, 29–35]. In mathematical terms, a fractal is a subset of Euclidean space characterized by a fractal dimension higher than its topological dimension, as introduced by Mandelbrot in 1983 [29, 30, 36, 37]. Using fractal geometry, the self-similarity and space-filling properties of dynamical systems can be extracted [38]. Time-series data can be classified as fractal or mono-fractal if it can be characterized by a single scaling exponent or as a linear function of moments. The presence of these scale-free databases has been observed in various fields, including biology, geophysics, stock markets, and finance [30, 39–45]. To analyze the nonlinear structure of scale-free time-series data effectively, it is essential to employ analytical and computational tools that can characterize their complexity and self-similarity [41, 46]. Traditional time-series analysis methods may fail when dealing with datasets exhibiting a wide range of scaling features. For such

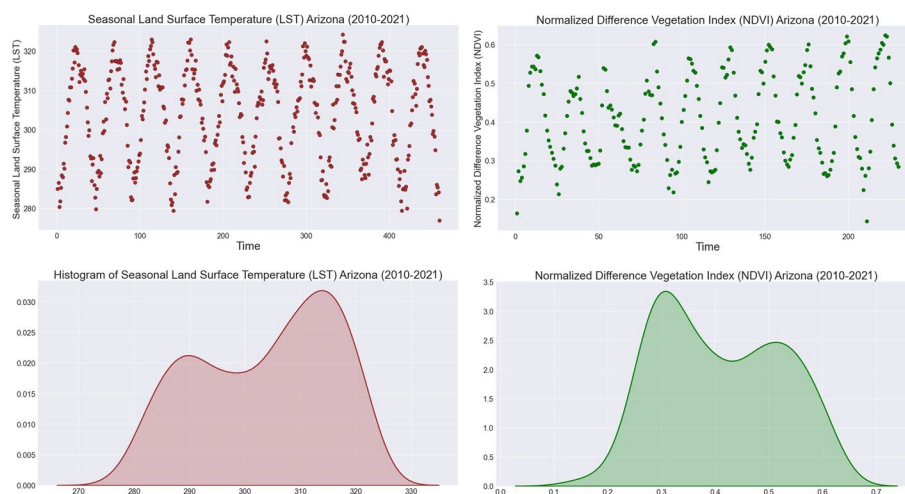


Fig. 2 Right up: Normalized Difference Vegetation Index (NDVI) Arizona versus time (2010–2021), Left up: Seasonal Land Surface Temperature (LST) Arizona versus time (2010–2021), Right down: the histogram of Normalized Difference Vegetation Index (NDVI) Arizona, Left down: the histogram of Seasonal Land Surface Temperature (LST) Arizona, <https://developers.google.com/earth-engine/datasets/catalog>; Google Earth Enterprise Open Source

Category	Historically observed impacts
D0	Forage crops and pasture are stressed; producers feed livestock early
	Ground is hard
	Agriculture ponds and creeks begin to decline
D1	Cash crop growth and yield are low
	National forests implement campfire and firework bans
	Streams and ponds are low
	Fire activity increases
D2	Crops are damaged, especially dryland corn
	Burn bans begin
	Large cracks appear in foundations of homes
	Large surface water levels drop; agricultural ponds and streams have dried up
	Saltwater intrusion occurs in rivers and bays; saltwater wildlife migrate upstream
D3	Hydroelectric power decreases; navigation is limited
	Soybean pods shatter
	Large-scale hay shortages occur; producers sell livestock
	Wildfire count and fire danger continue to increase
	Landscape growth is stunted and needs irrigation; Christmas tree growth is stunted
	Ground has noticeable cracks; road damage has occurred
	Low flow in rivers and lakes affects recreation
Water mains break daily in large municipalities; water conservation is implemented	
D4	Air quality is poor
	Trees and shrubs are defoliated; grass is brown; landscaping projects are delayed
	Wildfire count is very high
	Lakes are extremely low; large municipalities implement water restrictions; water prices increase

Fig. 3 Table of the reported impacts during past droughts in Arizona for each level of drought on the US Drought Monitor, <https://droughtmonitor.unl.edu/About/WhatistheUSDM.aspx>; (Source(s): National Drought Mitigation Center (NDMC), National Oceanic and Atmospheric Administration (NOAA), United States Department of Agriculture (USDA))

data, which may require multiple scaling exponents to describe their scaling structure, the scaling behavior follows a nonlinear function of moments (including vibration analysis using scaling power law and power spectral density (PSD) and continuous and discrete wavelet analysis) [47]. However, there exist other type processes which require a large number of scaling exponents to characterize their scaling structure. For this class of phenomena, the scaling behavior follows a function which is nonlinear in the moments. For these processes which are called multi-fractal, the variability in data exhibits self-affine multi-fractal properties and multi-fractal analysis needs to be applied to determine the complexity of consecutive time intervals in time-series data. In multi-fractal analysis, we discover whether some type of power-law scaling exists for various statistical moments at different scales [48–51].

In this novel study, we leverage the concept of fractal geometry to classify drought severity in the USA from 2000 to the present, recognizing the significance of drought characterization for future forecasting. Multi-fractal analysis is employed to investigate whether power-law scaling is present for various statistical moments at different scales in the dataset. By plotting multi-fractal spectra and applying quantitative analysis through the fractal dimension (FD) using the Higuchi algorithm, we illustrate the

fractal complexity of drought severity. Our findings suggest that fractal geometry can serve as a mathematical framework for the analysis and characterization of drought severity at different levels, offering a computational tool for comparing the complexity of each class of drought severity, ultimately aiding in predicting future drought occurrences.

2 Materials, methods, and results

2.1 Data

Here, data has been taken using "Drought Monitor" from all US Drought Monitor categories for each week of the selected time period (January 2000 to Nov 2021) and location (contiguous USA), see Figs. 4 and 5. The US Drought Monitor which started from 1999, is a partnership between the National Drought Mitigation Center (NDMC) at the University of Nebraska-Lincoln, the United States Department of Agriculture (USDA), and the National Oceanic and Atmospheric Administration (NOAA). Each Thursday, the US Drought Monitor (USDM) will be updated to demonstrate the location and intensity of drought across the country. Using the experts' assessments, drought categories display conditions related to dryness and drought such as observations of how much water is available in streams, lakes, and soils compared to usual time of year (Source(s): National Drought Mitigation Center (NDMC), National Oceanic and Atmospheric Administration (NOAA), United States Department of Agriculture (USDA)) [52].

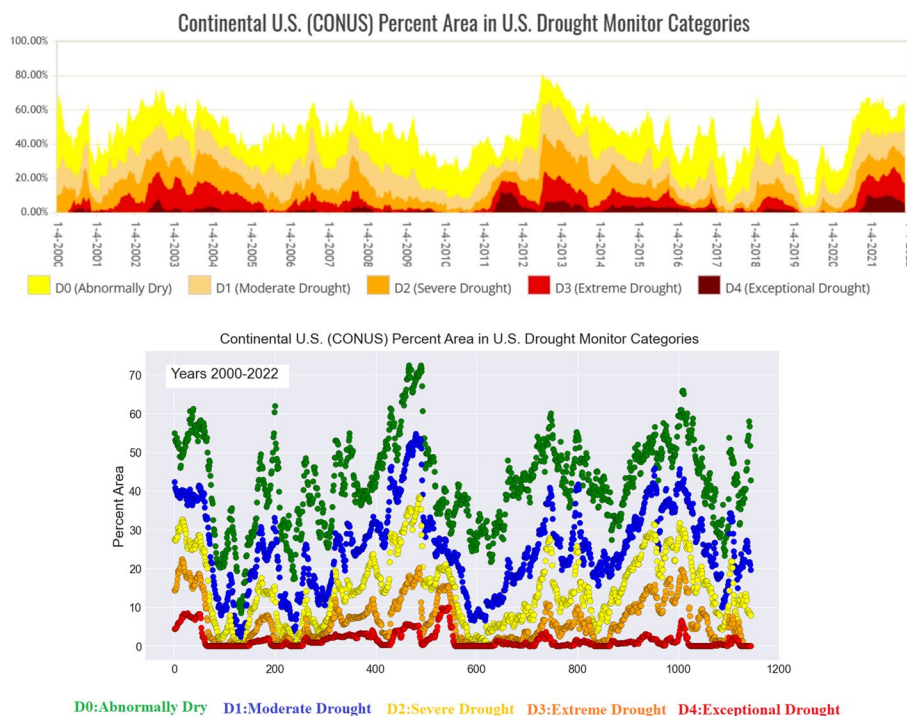
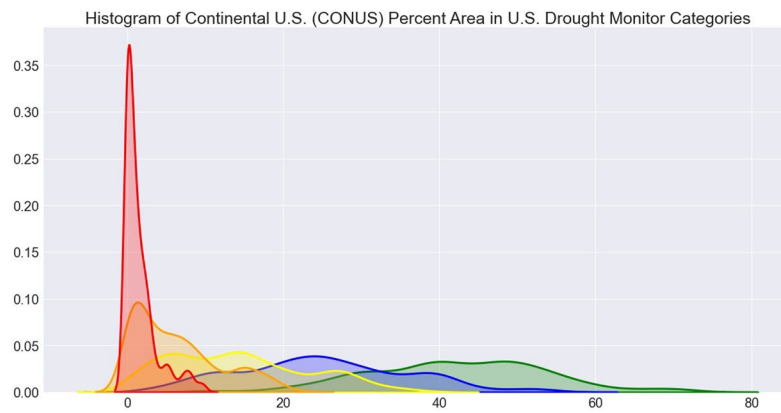


Fig. 4 Continental US (CONUS) Percent Area in US Drought Monitor Categories database (2000–present), the drought status of areas represented by points; Source(s): National Drought Mitigation Center (NDMC), the US Department of Agriculture (USDA), and the National Oceanic and Atmospheric Administration (NOAA), <https://droughtmonitor.unl.edu/DmData/TimeSeries.aspx>



D0:Abnormally Dry **D1:Moderate Drought** **D2:Severe Drought** **D3:Extreme Drought** **D4:Exceptional Drought**

Fig. 5 Histogram of Continental US (CONUS) Percent Area in US Drought Monitor Categories database (2000–present). The histogram uses five classifications: abnormally dry (D0), showing areas that may be going into or are coming out of drought, and four levels of drought: moderate (D1), severe (D2), extreme (D3) and exceptional (D4); Source(s): National Drought Mitigation Center (NDMC), the US Department of Agriculture (USDA), and the National Oceanic and Atmospheric Administration (NOAA)

2.2 Time–frequency analysis and continuous wavelet transform (CWT)

To represent non-stationary time-series databases, continuous wavelet transform (CWT) provides a clear visualization platform by computing a linear time–frequency called scalogram which breaks the dataset into scales by preserving time shifts and time scales. Therefore, when we are working with time-series data in different frequency ranges, the wavelet transform facilitates extracting useful information from the time intervals between consecutive waves of time series and makes analysis of data easier [53]. The continuous wavelet transform (CWT) of a dataset $h(t)$ is given by (Mallat, 1998) [53]

$$\text{CWT}(u, s) = \int_{-\infty}^{\infty} h(t) \frac{1}{|s|^{0.5}} \Phi^* \left(\frac{t-u}{s} \right) dt \quad (2.1)$$

where s is the scale, u is the displacement, Φ is the mother wavelet used, and $*$ means the complex conjugate. The CWT is therefore a convolution of the data with scaled version of the mother wavelet. Of course, the time coordinate t in Eq. (2.1) could equally well be the spatial coordinate x if profile data were being analyzed.

There is a propose a new classification method called wavelet transform-based smooth ordering (WTSO) which uses the WTSO wavelet transform to reduce the high dimensionality, the computational cost, and also perform classification [54]. In [55], the authors introduced a framework which performs better in downsampling balance and signal compression. Their wavelet decomposition method has application in application on synthetic and real-world graph. Another wavelet called Chebyshev wavelet has been used in fractional calculus and fractal geometry [56]. Guariglia et al. further developed mother wavelet in Taylor series using the differential properties of Chebyshev wavelets. Mallat et al. offered the wavelet representation as an orthogonal multiresolution representation which is defined between the spatial and Fourier domains [57]. In [58], the fractional derivative of the Gabor–Morlet wavelet has been used to obtain a characterization of the complex fractional derivative through the distribution theory. Sparse

representation by frames has shown promising results in signal analysis via a concise approach through practical numerical experiments [59].

2.3 Vibration frequency analysis using power spectral densities (PSD)

Discrete Fourier transform (DFT) or fast Fourier transform (FFT) is one of the most frequently used vibration frequency analysis algorithms in frequency analysis and computing Fourier transform. This method works very well when we have a finite number of dominant frequency components; however, it fails when our data includes random vibrations. To solve this problem, one may apply power spectral densities (PSD) technique which is perfect to analyze the signal vibration. The spectral densities (PSD) acts by multiplying each frequency bin of FFT to its complex conjugate to derive the real spectrum, and next, it normalizes the results to frequency bin width. Because the drought monitor database displays nonlinearity and has non-stationary structure, the welch (PSD) method with overlapped segmentation, which is an averaging estimator technique, has been applied to study the complex fluctuations in drought time-series structures.

2.4 Multi-fractal analysis and discrete wavelet transform (DWT)

There are different types of phenomena with scaling law behaviors which can be completely characterized using fractal theory. However, there exist some other processes which cannot be fully explained using fractal theory tools because they follow complex scaling behaviors of many irregular objects. For this group of phenomena, we may need to perform multi-fractal analysis which gives a spectrum of singularity exponents to describe the complex scaling behaviors. In general, fractal dimension determines the complexity of a fractal object by measuring the changes of coverings relative to the scaling factor. It also specifies the space-filling capacity of a fractal object with respect to its scaling properties in the space. The relationship between scaling and covering is often hard to be characterized. The variation in the number of coverings, $N(\epsilon)$, with respect to the scaling factor ϵ , can be written as

$$N(\epsilon) \propto \epsilon^{-D} \quad (2.2)$$

where D is the fractal dimension. Relation (2.2) is called scaling law that has been used to demonstrate the size distribution of many objects in nature. The box-counting formula which has been widely applied to approximate the fractal dimension of an irregular object is defined as

$$D_B = \lim_{a \rightarrow 0} \frac{\ln(N(a))}{\ln(1/a)} \quad (2.3)$$

However, this mono-fractal dimension is not able to fully characterize complex scaling behaviors of many irregular objects in the real world. That is why to study irregular objects like ECG signals one may need to apply the multi-fractal algorithm. The multi-fractal analysis used a spectrum of singularity exponents to provide a detailed and local description of complex scaling behaviors. In order to quantify local densities of the fractal set, we approximate the mass probability using the following formula

$$P_i(a) = \frac{N_i(a)}{N} \tag{2.4}$$

where $N_i(a)$ is the number of mass in the i th subset of measure a and N is the total mass of the set. When we scale the mass probability $P_i(a)$ with measure a of a multi-fractal set, it also demonstrates the power-law behavior:

$$P_i(a) \propto a^{\alpha_i} \tag{2.5}$$

where α_i is the singularity exponent characterizing the local scaling in the i th subset. The multi-fractal spectrum $f(\alpha)$ provides a statistical distribution of singularity exponents α_i . In general, $f(\alpha)$ may be estimated using the Legendre transformation

$$f(\alpha) = q \alpha - \tau(q) \tag{2.6}$$

$$\alpha(q) = \frac{d \tau(q)}{d q} \tag{2.7}$$

where q is the moment and $\tau(q)$ is the mass exponent of the q th order moment. In addition, the multi-fractal measures may be specified by scaling of q th moments of $P_i(a)$ as

$$\sum_{i=1}^{N(a)} P_i^{q(a)} \propto a^{\tau(q)} = a^{(q-1)D_q} \tag{2.8}$$

where $D_q = \frac{\tau(q)}{(q-1)}$ is the generalized fractal dimension. For $q = 0$, Eq. (2.4) becomes

$$N(a) \propto a^{-D_0} \tag{2.9}$$

which is similar to formula (2.2).

To approximate the multi-fractal spectrum, wavelet analysis has been used extensively with promising results for noisy time-series data [60–65]. This method utilizes discrete wavelet transform (DWT) technique which is robust enough to characterize the distribution of scaling exponents and provides a good approximation of the changes in regularity of data. The wavelet leader multi-fractal (WLM) analysis corresponds to the dimension of fractal sets to Holder exponent $\mathcal{H}(\tau)$ to quantify the spectrum of singularity of the point-wise regular function F [64]. The Holder exponent of a fractal process $F(\tau)$ is defined as follows:

Definition 2.1 [65] A fractal process $F(\tau)$ satisfies a Holder condition, when there exist $\mathcal{H}(\tau) > 0$, such that

$$|F(\tau_1) - F(\tau_2)| \simeq |\tau_1 - \tau_2|^{\mathcal{H}(\tau)} \tag{2.10}$$

We can find $\mathcal{H}(\tau)$ for constant F from the coarse Holder exponents as

$$h_\xi(\tau) = \frac{1}{\log \xi} \log \sup_{|\tau_1 - \tau_2| < \xi} |F(\tau_1) - F(\tau_2)| \tag{2.11}$$

The following sets have been introduced to discover the geometry of time-series data

$$\mathcal{E}_h^{[d]} = \{\tau : \mathcal{H}(\tau) = d\} \tag{2.12}$$

With varying d , these sets describe the local regularity of data. Next, we define the map

$$d \mapsto \dim(\mathcal{E}^{[d]}) \tag{2.13}$$

as the multi-fractal spectrum of F which is a compact form of the singularity structure of the fractal process [65]. To describe the complexity of time-series data in a global setting, we may need to count the intervals over which the fractal process F evolves with Holder exponent $\mathcal{H}(\tau)$ and it provides an estimation of $\dim(\mathcal{E}^{[d]})$. Then, we introduce the grain exponent which is a discrete approximation to $h_\xi(\tau)$ [65]:

$$h_k^{(n)} := -\frac{1}{n} \log_2 \sup\{|F(\eta) - F(\tau)| : (k - 1) 2^{-n} \leq \eta \leq \tau \leq (k + 2) 2^{-n}\} \tag{2.14}$$

Thus, the grain multi-fractal spectrum has the following form [66–69]

$$\mathcal{F}(d) = \lim_{\xi \rightarrow 0} \lim_{n \rightarrow \infty} \frac{\log \mathcal{N}^n(d, \xi)}{n \log 2} \tag{2.15}$$

where

$$\mathcal{N}^n(d, \xi) = \#\{k : |h_k^{(n)} - d| < \xi\} \tag{2.16}$$

2.5 Higuchi fractal dimension algorithm

Many different methods have been developed to measure the self-similarity of a fractal process. In fractal geometry, the Minkowski dimension or box-counting dimension is one of the most common used techniques to approximate the fractal dimension of a fractal set in any metric space [70]. However, this method cannot catch the sudden changes happen in the irregular time-series datasets [71]. To explore the complexity of scale-free time-series data, a variety of different nonlinear techniques such as Higuchi algorithm, power spectrum analysis, and Katz algorithm have been highlighted in different areas [72–77]. To approximate the complexity index of Drought Monitor Categories database, we utilize the Higuchi Algorithm [72]. We start with a finite time series $Y_1, Y_2, Y_3, \dots, Y_N$. Then, we build k new time series Y_m^k of the form

$$Y_m, Y_{m+k}, Y_{m+2k}, \dots, Y_{[m+Ak]} \tag{2.17}$$

where $A = (N - m)/k$. For each time interval k and the initial time m such that $m = 1, 2, \dots, k$, we calculate the length of Y_m^k using

$$L_m^k = \frac{\sum_{i=1}^{[A]} |Y_{m+ik} - Y_{m+(i-1)k}|}{k} R \tag{2.18}$$

where $R = (N - 1)/[A]k$ is the curve length normalization factor. Then, we estimate the mean of L_m^k for $m = 1, 2, \dots, k$ to find the average of curve length for each k . After finding the average values for $k = 1, \dots, k_{max}$, we plot $\log(L_m^k)$ versus $\log(1/k)$ for different time interval k . At the end, we calculate the slope of each regressed line. To find the

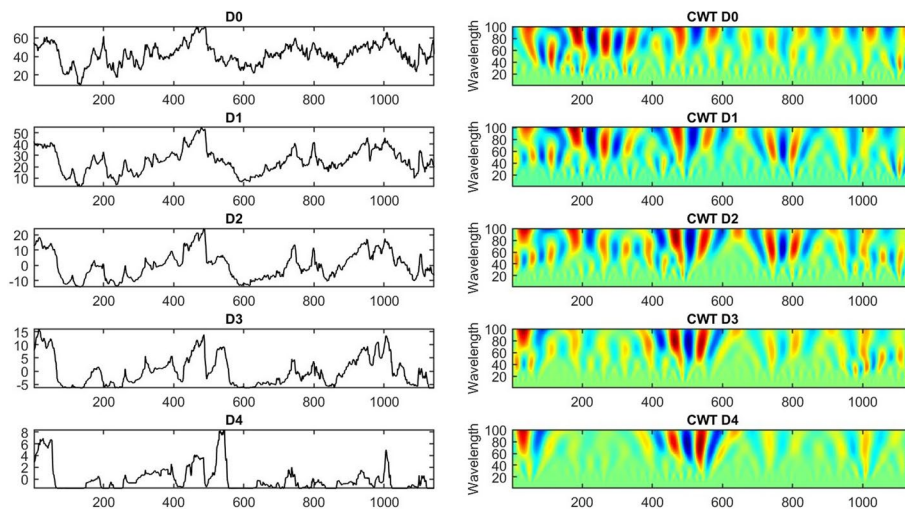


Fig. 6 Continuous wavelet transform (CWT) of Drought Monitor Categories database (2000–present) in time–wavelength space

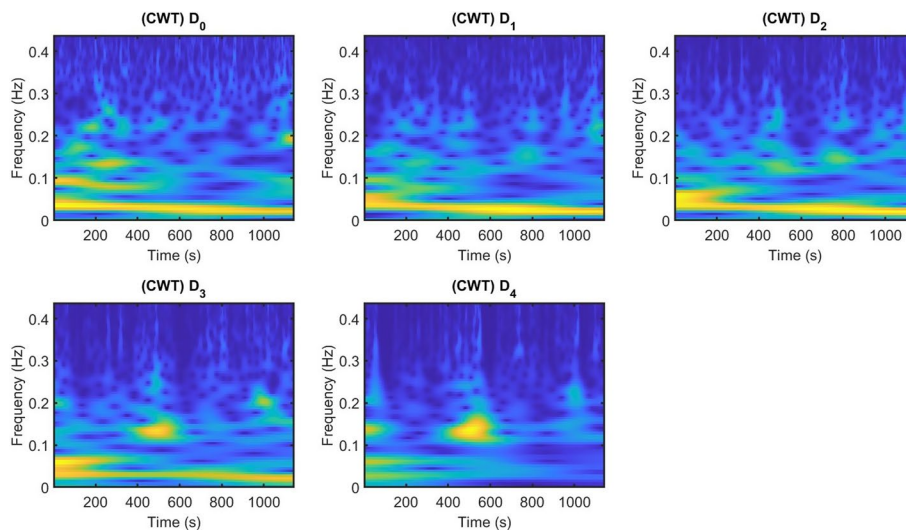


Fig. 7 Time–frequency representations of Drought Monitor Categories database (2000–present) using continuous wavelet transform (CWT) in two-dimensional time–frequency space

slope, we use the least squares approximation technique for an optimal value of time interval $k = 500$ when there is no change in fractal dimension after this value.

3 Discussion of results

Scalogram visualizes the dataset which is a function of time and frequency, by taking several steps: At first, it splits the data into overlapping segments, then computes the absolute value of the continuous wavelet transform coefficients for each segment, and finally plots it. We have demonstrated the continuous wavelet transform (CWT) plots of all drought categories database in Figs. 6, 7, and 8.

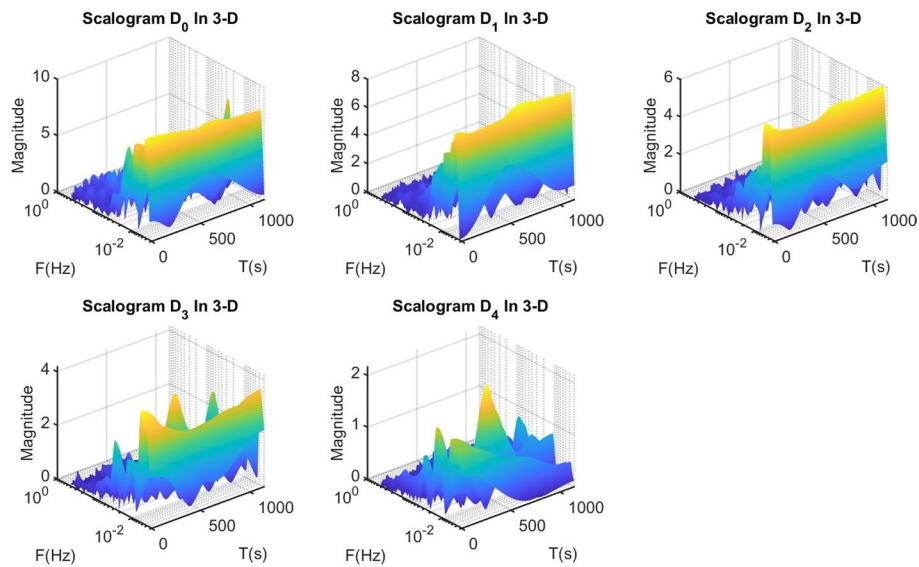


Fig. 8 Time–frequency representations of Drought Monitor Categories database (2000–present) using continuous wavelet transform (CWT) in three-dimensional time–frequency–magnitude space

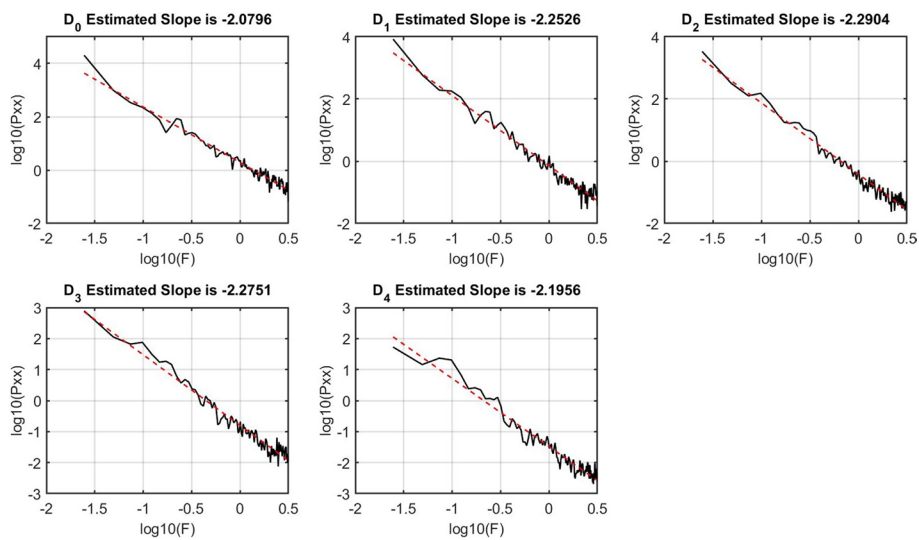


Fig. 9 Fitted least squares approximation to the logarithm of power spectral density of Drought Monitor Categories database (2000–present) obtained by wavelet techniques

Here, we can see the nonlinear features of the time-series data are encoded in the frequency domain of the vibrations.

To find whether for various statistical moments, power-law scaling behavior governs on the structure of the drought time-series data at different scales, we compute the power spectral density of each drought category time-series data using Welch (PSD) technique, and then, we use least square method to fit linear regression to the logarithm of power spectral density results. In Fig. 9, we can see the fitted least squares approximation to the logarithm of power spectral density of different drought categories. In fractal processes, there exists a scaling relationship between power and

frequency f in the spectral domain. These graphical representations in Fig. 9 reveal the fractal processes by a linear, negative slope of fitted least square lines, which means that the series cannot be generated by one or a finite set of subsystems, but for these processes different components act at different time scales. The results of power spectral density revealed the presence of long-range self-similar correlations extending over steps in a scale-free (fractal) power-law fashion. However, power spectral density fails to classify these five drought categories, and it may require to test this method with more databases.

Scaling exponent graphs are useful tools to demonstrate whether self-similar process is mono-fractal or multi-fractal. We also plot the scaling exponents of Drought Monitor Categories (2000–present) in Fig. 10. The nonlinear exponents for these signals may exhibit the multi-fractal structure of them; however, we need to apply multi-fractal analysis to check if this is a confirmed conclusion.

However, scaling exponent of Drought Monitor Categories does not give enough information to classify different drought categories for this limited database.

From multi-fractal analysis results (see Fig. 11), we can easily see that we have a wide range of exponents for extreme drought D_4 , which is a sign of multi-fractal structure of this drought level. This multi-fractal time-series data needs to be indexed by different exponents as we decompose it into different subsets and also requires much more exponents to characterize its scaling properties. In addition, we can find a clear loss of multi-fractality for abnormally dry to extreme drought $D_0 - D_3$, which means they are homogeneous and mono-fractal since their spectrum displays a narrow width of scaling exponent. Using multi-fractal analysis of drought time-series data, we can explore when moderate to extreme drought (D_1 or D_3) and exceptional drought (D_4) are present. Although multi-fractal analysis could well separate moderate to extreme drought from extreme drought and we could monitor the complexity of each drought category dataset in terms of mono-fractal and multi-fractality, these results do not give us a clear framework to differentiate D_0 , D_1 , D_2 , and D_3 from each other, and we need to find other tools and techniques to successfully classify different drought categories.

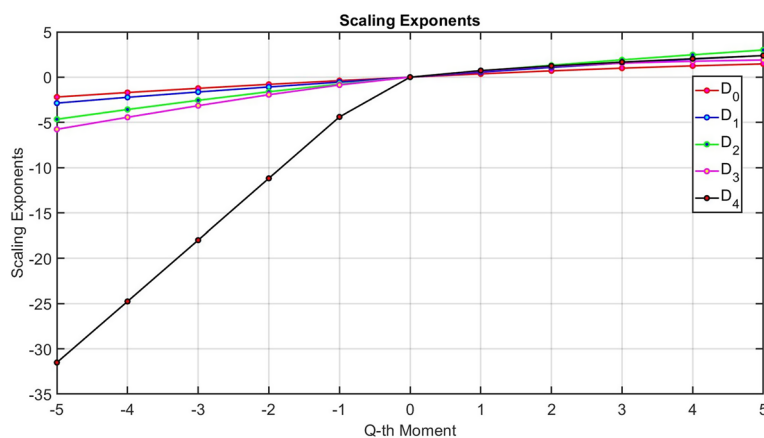


Fig. 10 Scaling exponent of power spectral density for Drought Monitor Categories database (2000–present)

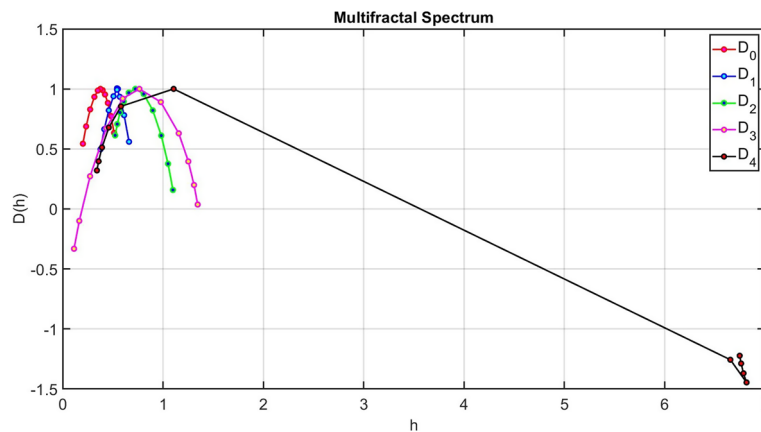


Fig. 11 The multi-fractal spectrum analysis of Drought Monitor Categories database (2000–present) shows the occurrence of multi-fractality with a broad range of exponents in data structure of D_4 and presence of mono-fractal behavior with a narrow range of exponent for $D_0 - D_3$

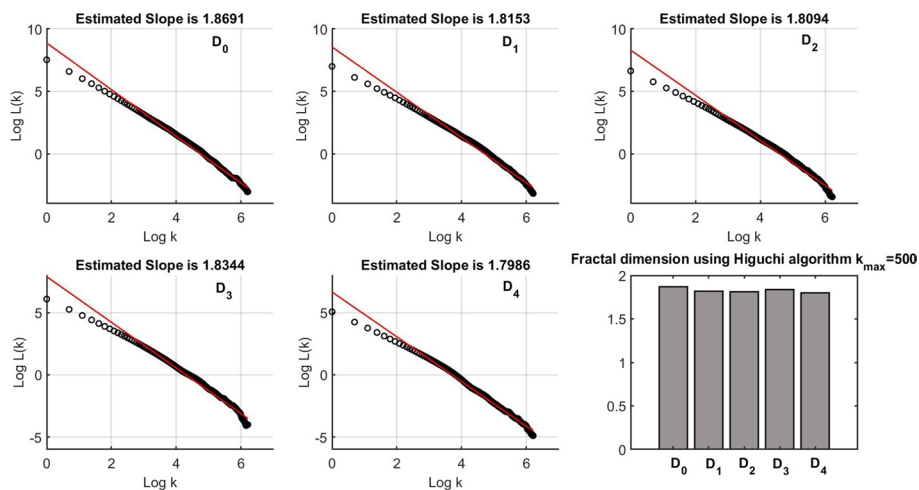


Fig. 12 Plots of $\log(L_m^k)$ versus $\log(k)$ for time interval $k = 500$, the logarithmic scale and the corresponding slope of fitted regression line (the Higuchi fractal dimension) for Drought Monitor Categories database (2000–present)

We have approximated the fractal dimension of Drought Monitor Categories database and plotted their regression models for each time series in Fig. 12.

From fractal dimension results in Fig. 12, we can compare the fractal dimension of different drought levels as

$$FD_{D_4} < FD_{D_2} < FD_{D_1} < FD_{D_3} < FD_{D_0} \tag{3.1}$$

Although fractal dimension using the Higuchi algorithm is a good index for comparing the self-similarity and power-law structures of different drought categories, it fails to separate these five groups of datasets, and also, we need to try different drought databases to find a threshold for classification of different levels of drought.

4 Conclusion

Drought, often perceived as a gradual and inconspicuous climatic phenomenon, has historically been underestimated in terms of its environmental and economic ramifications. However, once its profound impacts on the environment and the economy are recognized, it becomes evident that drought is as significant as fast-moving natural disasters like tornadoes and hurricanes. Therefore, efforts to comprehend and predict drought are of great importance and should be supported by relevant organizations.

In the USA, the National Integrated Drought Information System (NIDIS), a multi-agency partnership, is dedicated to enhancing drought monitoring, prediction, risk management, and planning at the national level. Given the substantial consequences of drought on agriculture, water supply, energy production, public health, and wildlife, our research aimed to identify analytical and computational techniques capable of classifying different drought severity levels using data from the US Drought Monitor database. Since this database displays irregular data structures, we opted for nonlinear techniques, such as vibration analysis and wavelet methods, specifically designed for this type of data. Our objective was to determine whether these techniques could effectively classify drought levels, ranging from moderate drought (D1) to exceptional drought (D4).

Our time–frequency analysis method, the continuous wavelet transform (CWT), successfully visualized the nonlinear structure of five distinct drought severity levels in the frequency domain of data oscillation. Utilizing the well-established vibration analysis techniques of power-law exponent and power spectral density, we uncovered power-law and self-similarity behaviors in the structure of the drought database. This discovery prompted us to proceed with fractal geometry techniques to further analyze the complexity of the various drought levels.

The nonlinear scaling exponents of the drought database suggested the presence of multi-fractality. Consequently, we conducted multi-fractal analysis using the discrete wavelet transform (DWT), a reputable method in time-series data analysis. The results showed a broad range of scaling exponents for exceptional drought (D4) and a narrower range for abnormally dry (D0) to severe drought (D3). This effectively differentiated the mono-fractal dynamics of these levels from the multi-fractal nature of exceptional drought (D4).

As a result, the wavelet leader multi-fractal (WLM) analysis can serve as a classifier method for distinguishing exceptional drought (D4) from other levels. However, it fails to differentiate between moderate drought (D1), severe drought (D2), and extreme drought (D3). To achieve a comprehensive understanding of complexity in drought time-series data, we conducted a fractal dimension analysis using the Higuchi algorithm, an appropriate technique for determining the fractal dimension of irregular, scale-free databases. The Higuchi fractal dimension revealed that abnormally dry (D0) had the highest fractal dimension, while exceptional drought (D4) had the lowest. Although it helped compare the self-similarity of different drought levels, this complexity index did not provide clear differentiation between the groups. Further analysis and effort are required to establish a specific threshold at which the fractal dimension can be considered a classification tool in such studies.

While the proposed algorithms have shown promising performance in various literature and evidence, a significant limitation lies in the limited amount of data available

from the existing online database. Moreover, understanding the mechanisms behind the long-range correlations in the complex fluctuations of drought data remains a challenge. Developing an appropriate mathematical model, whether deterministic or stochastic, to describe the complex dynamics of drought time-series data is essential. This endeavor calls for collaborative research between experimental and theoretical scientists to uncover effective strategies for forecasting drought and mitigating its impacts on the environment, wildlife, and the economy.

Abbreviations

D0	Abnormally dry
D1	Moderate drought
D2	Severe drought
D3	Extreme drought
D4	Exceptional drought
PSD	Power spectral densities
NDMC	National Drought Mitigation Center
NOAA	National Oceanic and Atmospheric Administration
USDA	United States Department of Agriculture
USDM	US Drought Monitor
NDVI	Normalized difference vegetation index
AVHRR	Advanced very-high-resolution radiometer
MODIS	Terra moderate resolution imaging spectroradiometer
LST	Land surface temperature
FD	Fractal dimension
CWT	Continuous wavelet transform
DFT	Discrete Fourier transform
FFT	Fast Fourier transform
WLM	Wavelet leader multi-fractal

Acknowledgements

We are deeply grateful to all those who played a role in the success of this project.

Funding

The author(s) received no financial support for the research.

Availability of data and materials

The data that support the findings of this study (Fig. 4) are available in/from US Drought Monitor Categories database (2000–present), the drought status of areas represented by points; Source(s): National Drought Mitigation Center (NDMC), the US Department of Agriculture (USDA), and the National Oceanic and Atmospheric Administration (NOAA), <https://droughtmonitor.unl.edu/DmData/TimeSeries.aspx>.

Declarations

Competing interests

The authors declare that they have no competing interests.

Received: 27 August 2023 Accepted: 6 December 2023

Published online: 02 January 2024

References

1. Y. Ding, M.J. Hayes, M. Widhalm, Measuring economic impacts of drought: a review and discussions. *Disaster Prev. Manag. Int. J.* **20**(4), 434–446 (2011)
2. R.A. Lawes, R.S. Kingwell, A longitudinal examination of business performance indicators for drought-affected farms. *Agric. Syst.* **106**(1), 94–101 (2012)
3. M. Alston, J. Kent, Social impacts of drought, in *Centre for Rural Social Research* (Charles Sturt University, Wagga Wagga, NSW, 2004)
4. L.M. Mosley, Drought impacts on the water quality of freshwater systems: review and integration. *Earth-Sci. Rev.* **140**, 203–214 (2015)
5. D.A. Wilhite, M.D. Svoboda, M.J. Hayes, Understanding the complex impacts of drought: a key to enhancing drought mitigation and preparedness. *Water Resour. Manag.* **21**(5), 763–774 (2007)
6. S. Azizi, T. Azizi, The fractal nature of drought: power laws and fractal complexity of Arizona drought. *Eur. J. Math. Anal.* **2**, 17 (2022)

7. M.M. Alimullah, Droughts in Asian least developed countries: vulnerability and sustainability. *Weather Climate Extremes* **7**, 8–23 (2015)
8. V.K. Vidyarthi, A. Jain, Knowledge extraction from trained ANN drought classification model. *J. Hydrol.* **585**, 124804 (2020)
9. Y. Yang, M. Anderson, F. Gao, C. Hain, A. Noormets, G. Sun, R. Wynne, V. Thomas, L. Sun, Investigating impacts of drought and disturbance on evapotranspiration over a forested landscape in North Carolina, USA using high spatiotemporal resolution remotely sensed data. *Remote Sens. Environ.* **238**, 111018 (2020)
10. S.R. Evett et al., Precision agriculture and irrigation: current US perspectives. *Trans. ASABE* **63**(1), 57–67 (2020)
11. M.S. Lisboa, R.L. Schneider, P.J. Sullivan, M.T. Walter, Drought and post-drought rain effect on stream phosphorus and other nutrient losses in the Northeastern USA. *J. Hydrol. Reg. Stud.* **28**, 100672 (2020)
12. R. Yaddanapudi, A.K. Mishra, Compound impact of drought and COVID-19 on agriculture yield in the USA. *Sci. Total Environ.* **807**, 150801 (2022)
13. D.J.N. Young, M. Meyer, B. Estes, S. Gross, A. Wuenschel, C. Restaino, H.D. Safford, Forest recovery following extreme drought in California, USA: natural patterns and effects of pre-drought management. *Ecol. Appl.* **30**(1), e02002 (2020)
14. N.T. Shephard, O. Joshi, C.R. Meek, R.E. Will, Long-term growth effects of simulated-drought, mid-rotation fertilization, and thinning on a loblolly pine plantation in southeastern Oklahoma, USA. *For. Ecol. Manag.* **494**, 119323 (2021)
15. M. Peña-Gallardo, S.M. Vicente-Serrano, F. Domínguez-Castro, S. Quiring, M. Svoboda, S. Beguería, J. Hannaford, Effectiveness of drought indices in identifying impacts on major crops across the USA. *Climate Res.* **75**(3), 221–240 (2018)
16. H. Wu, D.A. Wilhite, An operational agricultural drought risk assessment model for Nebraska, USA. *Nat. Hazards* **33**(1), 1–21 (2004)
17. J. Christian-Smith, M.C. Levy, P.H. Gleick, Maladaptation to drought: a case report from California, USA. *Sustain. Sci.* **10**(3), 491–501 (2015)
18. H. Chang, M.R. Bonnette, Climate change and water-related ecosystem services: impacts of drought in California, USA. *Ecosyst. Health Sustain.* **2**(12), e01254 (2016)
19. T. Tadesse, D.A. Wilhite, S.K. Harms, M.J. Hayes, S. Goddard, Drought monitoring using data mining techniques: a case study for Nebraska, USA. *Nat. Hazards* **33**(1), 137–159 (2004)
20. J.W. Nielsen-Gammon, The 2011 Texas drought. *Texas Water J.* **3**(1), 59–95 (2012)
21. B. Breyer, S.C. Zipper, J. Qiu, Sociohydrological impacts of water conservation under anthropogenic drought in Austin, TX (USA). *Water Resour. Res.* **54**(4), 3062–3080 (2018)
22. J.S. Clark, E.C. Grimm, J.J. Donovan, S.C. Fritz, D.R. Engstrom, J.E. Almendinger, Drought cycles and landscape responses to past aridity on prairies of the northern Great Plains, USA. *Ecology* **83**(3), 595–601 (2002)
23. I.W. Jung, H. Chang, Climate change impacts on spatial patterns in drought risk in the Willamette River Basin, Oregon, USA. *Theor. Appl. Climatol.* **108**(3), 355–371 (2012)
24. Y. Zhang, Z. Hao, Y. Jiang, V.P. Singh, Impact-based evaluation of multivariate drought indicators for drought monitoring in China. *Global Planetary Change* **228**, 104219 (2023)
25. R. Albarakat, V. Lakshmi, Comparison of normalized difference vegetation index derived from Landsat, MODIS, and AVHRR for the Mesopotamian marshes between 2002 and 2018. *Remote Sens.* **11**(10), 1245 (2019)
26. K.I. Wheeler, M.C. Dietze, A statistical model for estimating midday NDVI from the geostationary operational environmental satellite (GOES) 16 and 17. *Remote Sens.* **11**(21), 2507 (2019)
27. Y. Wang, C. Zhang, F.-R. Meng, C.P.-A. Bourque, C. Zhang, Evaluation of the suitability of six drought indices in naturally growing, transitional vegetation zones in Inner Mongolia (China). *PLoS ONE* **15**(5), e0233525 (2020)
28. C. Wu et al., An evaluation framework for quantifying vegetation loss and recovery in response to meteorological drought based on SPEI and NDVI. *Sci. Total Environ.* **906**, 167632 (2023)
29. B.B. Mandelbrot, *The Fractal Geometry of Nature*, vol. 1 (WH freeman, New York, 1982)
30. B.B. Mandelbrot, *Fractal Geometry and Applications: A Jubilee of Benoit Mandelbrot* (American Mathematical Society, Providence, 2004)
31. E. Guariglia, Harmonic Sierpinski gasket and applications. *Entropy* **20**(9), 714 (2018)
32. T. Azizi, Measuring fractal dynamics of FECG signals to determine the complexity of fetal heart rate. *Chaos Solitons Fractals X* **9**, 100083 (2022)
33. T. Azizi, On the fractal geometry of different Heart rhythms. *Chaos Solitons Fractals X* **9**, 100085 (2022)
34. T. Azizi, Mathematical modeling of stress using fractal geometry: the power laws and fractal complexity of stress. *Adv. Neurol. Neurosci.* **5**(3), 140–148 (2022)
35. S. Azizi, T. Azizi, Noninteger dimension of seasonal land surface temperature (LST). *Axioms* **12**(6), 607 (2023)
36. K. Falconer, *Fractal Geometry: Mathematical Foundations and Applications* (Wiley, New York, 2004)
37. J. Briggs, *Fractals: The Patterns of Chaos: A New Aesthetic of Art, Science, and Nature* (Simon and Schuster, New York, 1992)
38. E. Guariglia, Primality, fractality, and image analysis. *Entropy* **21**(3), 304 (2019)
39. M. Meyer, O. Stiedl, Self-affine fractal variability of human heartbeat interval dynamics in health and disease. *Eur. J. Appl. Physiol.* **90**(3), 305–316 (2003)
40. R. Acharya, P.S. Bhat, N. Kannathal, A. Rao, C.M. Lim, Analysis of cardiac health using fractal dimension and wavelet transformation. *Itbm-Rbm* **26**(2), 133–139 (2005)
41. R. Martin, Noise power spectral density estimation based on optimal smoothing and minimum statistics. *IEEE Trans. Speech Audio Process.* **9**(5), 504–512 (2001)
42. A.J. Barbour, R.L. Parker, psd: Adaptive, sine multitaper power spectral density estimation for R. *Comput. Geosci.* **63**, 1–8 (2014)
43. S. Di Matteo, N.M. Viall, L. Kepko, Power spectral density background estimate and signal detection via the multitaper method. *J. Geophys. Res. Space Phys.* **126**(2), e2020JA028748 (2021)

44. C. Heneghan, G. McDarby, Establishing the relation between detrended fluctuation analysis and power spectral density analysis for stochastic processes. *Phys. Rev. E* **62**(5), 6103 (2000)
45. T. Di Matteo, Multi-scaling in finance. *Quant. Finance* **7**(1), 21–36 (2007)
46. P. Laguna, G.B. Moody, R.G. Mark, Power spectral density of unevenly sampled data by least-square analysis: performance and application to heart rate signals. *IEEE Trans. Biomed. Eng.* **45**(6), 698–715 (1998)
47. C.-K. Peng, S. Havlin, H.E. Stanley, A.L. Goldberger, Quantification of scaling exponents and crossover phenomena in nonstationary heartbeat time series. *Chaos Interdiscip. J. Nonlinear Sci.* **5**(1), 82–87 (1995)
48. I.P. Ch, L.A.N. Amaral, A.L. Goldberger, S. Havlin, M.G. Rosenblum, Z.R. Struzik, H.E. Stanley, Multifractality in human heartbeat dynamics. *Nature* **399**(6735), 461–465 (1999)
49. R. Sassi, M.G. Signorini, S. Cerutti, Multifractality and heart rate variability. *Chaos Interdiscip. J. Nonlinear Sci.* **19**(2), 028507 (2009)
50. D.C. Lin, A. Sharif, Common multifractality in the heart rate variability and brain activity of healthy humans. *Chaos Interdiscip. J. Nonlinear Sci.* **20**(2), 023121 (2010)
51. V. Tamas, Fractal growth phenomena. *Asakura Shoten* (1992)
52. M. Svoboda, D. LeComte, M. Hayes, R. Heim, K. Gleason, J. Angel, B. Rippey, R. Tinker, M. Palecki, D. Stooksbury, The drought monitor. *Bull. Am. Meteorol. Soc.* **83**(8), 1181–1190 (2002)
53. S. Mallat, *A Wavelet Tour of Signal Processing* (Elsevier, Amsterdam, 1999)
54. L. Yang, H. Su, C. Zhong, Z. Meng, H. Luo, X. Li, Y.Y. Tang, Y. Lu, Hyperspectral image classification using wavelet transform-based smooth ordering. *Int. J. Wavelets Multiresolut. Inf. Process.* **17**(06), 1950050 (2019)
55. X. Zheng, Y.Y. Tang, J. Zhou, A framework of adaptive multiscale wavelet decomposition for signals on undirected graphs. *IEEE Trans. Signal Process.* **67**(7), 1696–1711 (2019)
56. E. Guariglia, R.C. Guido, Chebyshev wavelet analysis. *J. Funct. Spaces* (2022). <https://doi.org/10.1155/2022/5542054>
57. S.G. Mallat, A theory for multiresolution signal decomposition: the wavelet representation. *IEEE Trans. Pattern Anal. Mach. Intell.* **11**(7), 674–693 (1989)
58. E. Guariglia, S. Silvestrov, *Fractional-Wavelet Analysis of Positive definite Distributions and Wavelets on $D'(C) D'(C)$* (Springer, Berlin, 2016), pp.337–353
59. C. Baker, Sparse representation by frames with signal analysis. *J. Signal Inf. Process.* **7**(1), 39–48 (2016)
60. L. Rodríguez-Liñares, A.J. Méndez, M.J. Lado, D.N. Olivieri, X.A. Vila, I.V. Gómez-Conde, An open source tool for heart rate variability spectral analysis. *Comput. Methods Programs Biomed.* **103**(1), 39–50 (2011)
61. H. Wendt, P. Abry, Multifractality tests using bootstrapped wavelet leaders. *IEEE Trans. Signal Process.* **55**(10), 4811–4820 (2007)
62. H. Wendt, P. Abry, S. Jaffard, Bootstrap for empirical multifractal analysis. *IEEE Signal Process. Mag.* **24**(4), 38–48 (2007)
63. S. Jaffard, B. Lashermes, P. Abry, *Wavelet Analysis and Applications* (Springer, Berlin, 2006), pp. 201–246
64. S. Jaffard, Wavelet techniques in multifractal analysis. *PARIS UNIV (FRANCE)*, (2004)
65. R.H. Riedi, Multifractal processes. *Rice Univ Houston Tx Dept Of Electrical And Computer Engineering*, (1999)
66. B.B. Mandelbrot, Possible refinement of the lognormal hypothesis concerning the distribution of energy dissipation in intermittent turbulence, in *Statistical Models and Turbulence*. Springer, pp 333–351 (1972)
67. R. Riedi, An improved multifractal formalism and self-similar measures. *J. Math. Anal. Appl.* **189**(2), 462–490 (1995)
68. H.G.E. Hentschel, I. Procaccia, The infinite number of generalized dimensions of fractals and strange attractors. *Physica D Nonlinear Phenomena* **8**(3), 435–444 (1983)
69. T.C. Halsey, M.H. Jensen, L.P. Kadanoff, I. Procaccia, B.I. Shraiman, Fractal measures and their singularities: the characterization of strange sets. *Phys. Rev. A* **33**(2), 1141 (1986)
70. C. Panigrahy, A. Garcia-Pedrero, A. Seal, D. Rodríguez-Esparragón, N.K. Mahato, C. Gonzalo-Martín, An approximated box height for differential-box-counting method to estimate fractal dimensions of gray-scale images. *Entropy* **19**(10), 534 (2017)
71. Y. Öztürk, Fractal Dimension as a Diagnostic Tool for Cardiac Diseases (2019)
72. T. Higuchi, Approach to an irregular time series on the basis of the fractal theory. *Physica D Nonlinear Phenomena* **31**(2), 277–283 (1988)
73. E. Shamsi, M.A. Ahmadi-Pajouh, T.S. Ala, Higuchi fractal dimension: an efficient approach to detection of brain entrainment to theta binaural beats. *Biomed. Signal Process. Control* **68**, 102580 (2021)
74. R.S. Gomolka, S. Kampusch, E. Kaniusas, F. Thürk, J.C. Széles, W. Klonowski, Higuchi fractal dimension of heart rate variability during percutaneous auricular vagus nerve stimulation in healthy and diabetic subjects. *Front. Physiol.* **9**, 1162 (2018)
75. M.J. Katz, Fractals and the analysis of waveforms. *Comput. Biol. Med.* **18**(3), 145–156 (1988)
76. A. Gil, V. Glavan, A. Wawrzaszek, R. Modzelewska, L. Tomasiak, Katz fractal dimension of geoelectric field during severe geomagnetic storms. *Entropy* **23**(11), 1531 (2021)
77. T. Azizi, On the fractal geometry of gait dynamics in different neuro-degenerative diseases. *Phys. Med.* **14**, 100050 (2022)

Publisher's Note

Springer Nature remains neutral with regard to jurisdictional claims in published maps and institutional affiliations.